transmissivity and reflectivity, when the average value of albedo is used instead of the actual variation of albedo within the medium. To investigate this matter, we consider several different spacial variations of albedo within the medium such that for each case the average value of $\omega(x)$ over the medium is equal to $\omega_{ave} = 0.5$. Table 1 lists the results obtained from such calculations for both linear and quadratic variations of albedo for an optical thickness of $a = 1$. It appears that the reflectivity of the slab varies significantly with the variation in the distribution of $\omega(x)$, whereas the change in transmissivity is very small. For example, for the case of $\omega(x) = x$ and isotropic incidence, the use of arithmetic average for ω overestimates reflectivity about 107%, but the transmissivity is underestimated only by about 2%. In the case of normal incidence, these errors are 68 and 4%, respectively.

This same trend continues for all optical thicknesses as shown in Fig. 1. The transmissivity curves are very close to each other indicating a weak dependence of transmissivity on the spacial variation of albedo. As expected, the transmissivity approaches zero as the optical thickness becomes larger. On the other hand the reflectivity curves for $\omega(x) = x/a$ and $\omega(x) = 1 - x/a$ are far apart from each other, especially at larger optical thicknesses, indicating strong dependence of reflectivity on the spacial distribution of the albedo. A similar trend is apparent for the case of normal incidence as shown in Fig. 1(b).

The present approach is also applicable for the exponential variation of albedo in the form $\omega(x) = \omega_0 e^{-x/s}$, if the exponential function is represented by its polynomial expansion. This is demonstrated by comparing our results with those obtained in ref. [1] using the F_N method, for the case of $s = 100$. We used the first ten terms of the polynomial expansion of the exponential function, which involves an error less than 10^{-16} in albedo for $a \leqslant 10$. The agreement between the two results was excellent.

In Table 2, we present the angular distribution of radiation intensity for $\omega(x) = x/a$ at three different locations in the medium (i.e. at $x = 0$, $a/2$ and a) for different optical thicknesses for the cases of both isotropic and normal incidence. Here we list in the last column the number of terms, NT, used in the expansion to achieve convergence for a specified degree of accuracy. The functional form of the albedo, $\omega(x)$, did not seem to have much effect on the number of terms required to achieve a specified accuracy.

Acknowledgement—This work was supported in part by the National Science Foundation through a grant MEA 81-10705.

REFERENCES

1. R. D. M. Garcia and C. E. Siewert, Radiative transfer in finite inhomogeneous plane-parallel atmospheres, *J. Quantve Spectrosc. Radiat. Transfer* **27**(2), 141–148 (1982).
2. Y. A. Cengel, M. N. Özişik and Y. Yener, Determination of angular distribution of radiation in an isotropically scattering slab, ASME Paper No. 83-HT-34 (1983).
3. M. N. Özişik, *Radiative Transfer*. Wiley, New York (1973).

Int. J. Heat Mass Transfer. Vol. 27, No. 10, pp. 1922–1925, 1984
Printed in Great Britain

0017-9310/84 $3.00 + 0.00

Effect of inert regions on local mass transfer rate measurements using the limiting diffusion current technique—case of Poiseuille type flow

HO NAM CHANG,† JOONG KON PARK and CHEOL KIM
Department of Chemical Engineering, Korea Advanced Institute of Science and Technology, P.O. Box 150 Chongyang, Seoul, Korea

(*Received* 2 *September* 1983 *and in revised form* 12 *January* 1984)

NOMENCLATURE

- c concentration
- D diffusion coefficient
- H height of the channel
- h grid size, x-direction
- k grid size, y-direction
- L length of the nonconducting segment
- Pe Peclet number, $(Re\ Sc) = Hu_{av}/D$
- R length of conducting region/length of nonconducting region
- Sc Schmidt number, $\mu/\rho D$
- u velocity
- u_{av} average velocity
- x, y x-, y-coordinate.

Superscript
- * dimensionless quantity represented by equation (5).

1. INTRODUCTION

MOST widely used in recent years for fluid–solid mass transfer studies is the limiting current technique, which measures a current density at a cathode where reduction of ferricyanide takes place. The details of the limiting current technique may be found elsewhere [1–3].

In order to understand local characteristics of mass transfer around the solid surface it becomes necessary to measure local

† To whom all correspondence should be addressed.

mass transfer rates. This can be accomplished with segmented electrodes using the limiting current technique. This technique has been successfully employed for exploring axial local wall mass transfer distribution downstream of a nozzle wall [4, 5] in measuring the circumferential distribution of local Sherwood number in a semi-cylindrical hollow oriented transverse to the main flow [6], and in studying the effect of turbulence promoters on local mass transfer [7, 8]. The use of this method requires that the electrodes be electrically isolated from one another. Accordingly, the regions between electrodes become electrically inert. Since electrochemical reaction is absent in these inert regions, the concentration of ions at the inert surface increases and thus the distribution of local mass transfer coefficients at the next electrodes are measured larger than those with the continuous electrodes. In order to analyze this effect mathematically a system of parallel plates is chosen and the local Sherwood number in each segment is numerically calculated and compared. The results of this study reveal the errors introduced due to the segmentation of electrodes.

2. MASS TRANSFER ON THE SEGMENTED ELECTRODES

For simplicity of the problem we have chosen the two-dimensional geometry with plane parallel plates shown in Fig. 1. The strip electrodes are embedded on the upper and lower walls and spaced at regular intervals. For the velocity profile fully developed Poiseuille flow is assumed. The ratio of channel length to channel height (H) is assumed to be large, as is usually the case in practice. The Peclet number is very large, which assumes that the thickness of the concentration boundary layer is much thinner than the channel height. Under the above assumptions the mass transfer equation can be written as

$$u\frac{\partial c}{\partial x} = D\frac{\partial^2 c}{\partial y^2} \tag{1}$$

$$u = 6u_{av}\left(\frac{y}{H} - \frac{y^2}{H^2}\right) \tag{2}$$

and the boundary conditions are given as

$$x = 0, \quad c = c_0$$

$$y = 0, \quad c = 0 \quad \text{for conducting region}$$

$$\frac{\partial c}{\partial y} = 0 \quad \text{for nonconducting region}$$

$$y = \frac{H}{2}, \quad \frac{\partial c}{\partial y} = 0. \tag{3}$$

Also we define the ratio of the conducting region to the nonconducting region as

$$R = \frac{\text{length of conducting region}}{\text{length of nonconducting region}}. \tag{4}$$

The following dimensionless variables and parameters are defined

$$u^* = \frac{u}{u_{av}}, \quad x^* = \frac{x}{(H\,Pe)}, \quad y^* = \frac{y}{H}, \quad c^* = \frac{c}{c_0},$$
$$Pe = Re \quad Sc = Hu_{av}/D. \tag{5}$$

In terms of these dimensionless variables equations (1)–(3) become

$$u^*\frac{\partial c^*}{\partial x^*} = \frac{\partial^2 c^*}{\partial y^{*2}} \tag{6}$$

$$u^* = 6y^*(1-y^*) \tag{7}$$

$$x^* = 0, \quad c^* = 0 \quad \text{for conducting region}$$

$$\frac{\partial c^*}{\partial y^*} = 0 \quad \text{for nonconducting region}$$

$$y^* = \frac{1}{2}, \quad \frac{\partial c^*}{\partial y^*} = 0. \tag{8}$$

3. METHOD OF THE SOLUTION

Using the Crank–Nicolson formula equation (6) is written in finite-difference form

$$u^*_{i,j}\frac{c^*_{i+1,j} - c^*_{i,j}}{h} = \frac{1}{k^2}$$
$$\times\{\tfrac{1}{2}(c^*_{i,j+1} - 2c^*_{i,j} + c^*_{i,j-1}) + \tfrac{1}{2}(c^*_{i+1,j+1} - 2c^*_{i+1,j} + c^*_{i+1,j-1})\}$$
$$u^*_{i,j} = 6k^2 j(1-j) \tag{9}$$

where i, j refer to the ith and jth nodes at the x and y axes, respectively. If we let the length of the nonconducting region be L, the same boundary conditions at $y = 0$ are given for the conducting and nonconducting regions alternately. The dimensionless interval P is given by

$$P = \frac{(R+1)L}{H\,Pe} \tag{10}$$

and the boundary conditions are

$$\text{at } x^* = 0, \quad c^*_{0,j} = 1$$

$$\text{at } y^* = 0, \quad c^*_{i,0} = 0$$

$$for\ (n-1)P < x^* < \left(n-1+\frac{R}{R+1}\right)P$$

(conducting region)

$$\text{at } y^* = \frac{1}{2}, \quad c^*_{i,j-1} = c^*_{i,j+1}$$

$$\text{for } \left(n-1+\frac{R}{R+1}\right)P < x^* < nP.$$

(nonconducting region) (11)

The numerical solutions for equations (9)–(11) are easily obtained by the Thomas algorithm [9]. The local Sherwood number is calculated as

$$Sh = \left.\frac{\partial c^*}{\partial y^*}\right|_{y^*=0} = \frac{1}{h}(c^*_{i,1} - c^*_{i,0}). \tag{12}$$

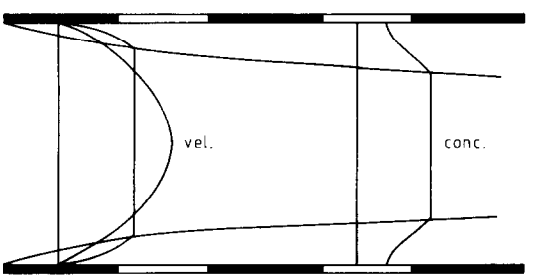

FIG. 1. Distributions of concentration and velocity in the conducting–nonconducting parallel plates.

4. RESULTS AND DISCUSSION

Here we considered the case for $Pe \gg 1$ which is very often encountered in most mass transfer studies. The solution was obtained up to $x^* = 60 \times 10^{-5}$.

Figure 2 shows the comparison of the local mass transfer rates between the nonsegmented electrode ($R = \infty$), and the segmented electrodes with $R = 10$ and 2. The local mass transfer rate on the nonsegmented electrode is infinite at the beginning but decreases rapidly due to the depletion of electrolyte at the electrode surface. In other terms it is said that the mass transfer rate drops due to the growth of the concentration boundary layer. This is the typical solution of the Graetz-type problem in mass transfer. In the case of $R = 2$ the drop is not continuous. The local mass transfer rate is denoted by the Sherwood number. Initially Sh is the same as that for the nonsegmented case, but at the second electrode a distance L from the first the peak Sh is lower than at the first electrode, but it is higher than the Sh at the end of the first electrode. This means that the electrolyte moved towards the surface while it passed over the inert region, which resulted in the buildup of nonzero concentration at the inert region surface (Fig. 4). However, the elevated peak Sh at each electrode decreased depending on the distance from the entrance region. In the case of $R = 10$ the profile is very close to that of $R = \infty$ as expected.

Figure 3 shows the mass transfer boundary layer thickness defined as $c^*(\delta) = 0.99$ in this study. Despite the discrepancy in mass transfer rates on segmented electrodes, the variation in boundary layer thickness is rather small. This reflects the fact that ions near the electrode surface move in to increase the electrolyte concentration near the electrode surface since the electrolytes are not depleted while they pass over the inert regions.

Figure 4 shows the concentration profile over the segmented electrode ($R = 5$). The concentration at $y^* = 0$ on the inert region is not zero, which gives elevated mass transfer rates at the next electrode.

Finally Table 1 summarizes the discrepancies in mean Sherwood number using the segmented electrodes. As R increases, the discrepancy between the nonsegmented and segmented electrodes decreases. For instance, in the case of $R = 5$, the discrepancy is about 15% and $R = 10$ gives a discrepancy of less than 8%. These errors seem quite insensitive to the location of the electrodes. As a conclusion it is

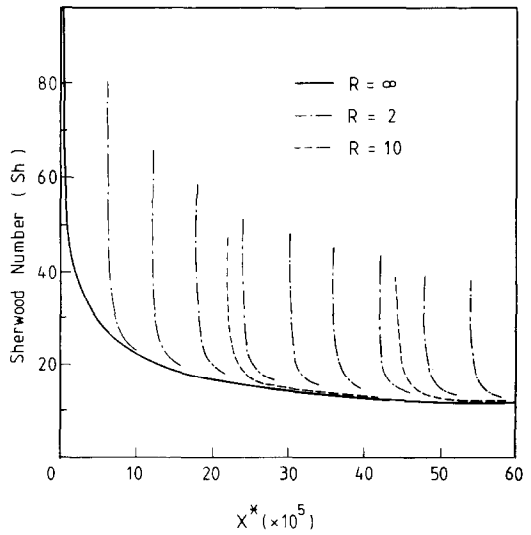

FIG. 2. Sherwood number distributions in the conducting–nonconducting parallel plates ($H\,Pe/L = 50\,000$).

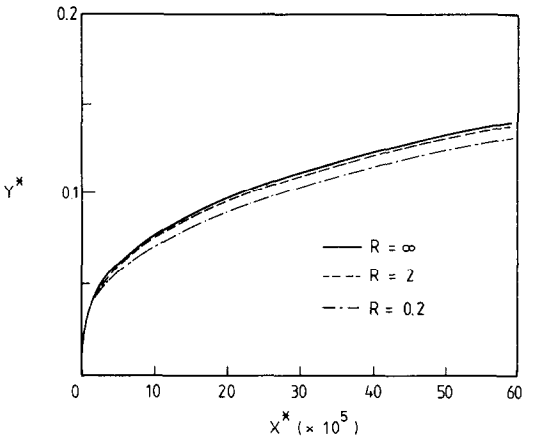

FIG. 3. Concentration boundary layer thickness ($H\,Pe/L = 50\,000$).

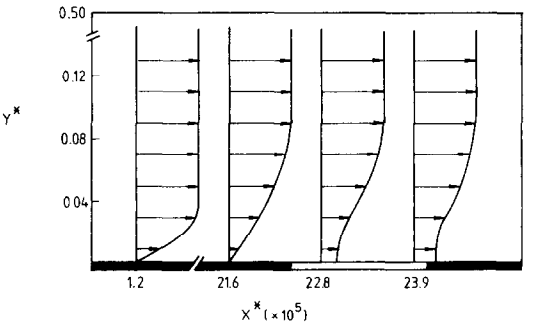

FIG. 4. Distributions of concentration ($R = 5$, $H\,Pe/L = 50\,000$).

Table 1. Percentage error of mean Sherwood number across one conducting region, compared to that at $R = \infty$†

Region No.	$R = 1$	$R = 2$	$R = 5$	$R = 10$
1	0	0	0	0
3	47.9	29.1	14.0	7.7
5	56.1	32.7	15.1	8.0
7	60.4	35.7	15.5	—
9	63.1	36.5	15.8	—
11	65.1	37.1	—	—
13	66.7	37.6	—	—
15	67.9	38.0	—	—
17	68.8	38.4	—	—
19	69.7	—	—	—
21	70.5	—	—	—
25	71.8	—	—	—
29	72.7	—	—	—

† Note: the percentage error was calculated according to the following equation

$$(\%\ \text{error}) = 100 \times (Sh_m(R) - Sh_m(\infty))/Sh_m(\infty).$$

important to estimate the errors introduced using segmented electrodes in measuring local mass transfer rates.

Acknowledgement—The authors are indebted to the Korea Science and Engineering Foundation (KOSEF) for partial support of this research.

REFERENCES

1. C. S. Lin, E. B. Denton, H. S. Gaskill and G. L. Putnam, Diffusion-controlled electrode reactions, *Ind. Engng Chem.* **43,** 2136–2143 (1951).
2. L. P. Reiss and T. J. Hanratty, Measurement of instantaneous rates of mass transfer to a small sink on a wall, *A.I.Ch.E. Jl* **8,** 245–247 (1962).
3. P. P. Grassman, Application of the electrolytic method—I. Advantages and disadvantages, mass transfer between a falling film and the wall, *Int. J. Heat Mass Transfer* **22,** 795–798 (1979).
4. D. J. Tagg, M. A. Patrick and A. A. Wragg, Heat and mass transfer downstream of abrupt nozzle expansions in turbulent flow, *Trans. Instn Chem. Engrs* **57,** 176–181 (1979).
5. A. A. Wragg, D. J. Tagg and M. A. Patrick, Diffusion controlled current distributions near cell entries and corners, *J. Appl. Electrochem.* **10,** 43–47 (1980).
6. J. K. Aggarwal and L. Talbot, Electro-chemical measurements of mass transfer in semi-cylindrical hollows, *Int. J. Heat Mass Transfer* **22,** 61–75 (1979).
7. P. H. Bradley, J. L. Greatorex and F. B. Leitz, Effect of turbulence promoters on local mass transfer, OSW contract No. 14-01-0001-2174 (1970).
8. D. H. Kim, I. H. Kim and H. N. Chang, Experimental study of mass transfer around a turbulence promoter by the limiting current method, *Int. J. Heat Mass Transfer* **26,** 1007–1016 (1983).
9. W. F. Ames, *Numerical Methods for Partial Differential Equations.* Academic Press, New York (1977).

Int. J. Heat Mass Transfer. Vol. 27, No. 10, pp. 1925–1928, 1984
Printed in Great Britain

0017–9310/84 $3.00 + 0.00

Non-uniform energy generation effects on natural convection in a spherical annulus enclosure

J. M. NELSEN† and R. W. DOUGLASS

Department of Mechanical Engineering, University of Nebraska, Lincoln, NE 68588-0525, U.S.A.

(*Received* 7 *February* 1983 *and in revised form* 10 *January* 1984)

NOMENCLATURE

$f(r)$ dimensionless generation rate function
g gravitational acceleration [m s^{-2}]
Gr Grashof number, $g\beta R_2^5\bar{Q}/kv^2$
k thermal conductivity of the fluid [W m^{-1} K^{-1}]
Pr Prandtl number, v/α
$q_w(\theta)$ local wall heat flux, $q_w^*/(R_2\bar{Q}) = (\partial T/\partial r)_1$ [W m^{-2}]
$\dot{q}(r)$ prescribed energy generation rate function, $\dot{Q}f(r)$ [W m^{-3}]
$\dot{Q}$ maximum value of $\dot{q}(r)$ [W m^{-3}]
$\bar{Q}$ volume averaged rate of energy released,

$$\frac{3\dot{Q}}{(1-\eta^3)}\int_\eta^1 f(r)r^2\,dr\ [\mathrm{W\,m^{-3}}]$$

r radial coordinate [m]
R_1, R_2 inner and outer sphere radii [m]
$T(r,\theta)$ temperature field [K]
T_2 outer sphere temperature.

Greek symbols
α thermal diffusivity of the fluid [m^2 s^{-1}]
β coefficient of volume expansion of the fluid [K^{-1}]
η radius ratio, R_1/R_2
θ latitudinal coordinate
v kinematic viscosity of the fluid [m^2 s^{-1}]
$\psi(r,\theta)$ stream function [m^3 s^{-1}].

Subscripts
$(\,)_r$ partial derivative with respect to r

Superscripts
$(\,)^*$ dimensional quantity.

INTRODUCTION

IN A RECENT paper Nelsen *et al.* [1] discussed natural convection in a spherical annulus driven by uniformly distributed energy generation within the annulus fluid. The purpose of this note is to extend those results to include radially non-uniform generation rate distributions in the annulus and to investigate their effect on the flow field. Under study is the steady buoyancy driven flow of a Boussinesq fluid within a concentric spherical annulus enclosure. The inner wall is insulated while the outer sphere is an isotherm (T_2). Such a configuration is of practical interest as discussed in ref. [1]. Of interest here, however, are the generic attributes of the apparatus as determined by an approximate numerical method, the method of partial spectral expansions.

MATHEMATICAL MODEL AND SOLUTION

A Boussinesq fluid fills a concentric spherical annulus enclosure whose inner radius is R_1 and outer radius is R_2. The fluid is generating energy at a prescribed rate, $\dot{q} = \dot{q}(r)$.

† Present address: Sandia National Laboratories, Albuquerque, NM 87185, U.S.A.